CARBON 50 (2012) 5085–5092

Available at www.sciencedirect.com

SciVerse ScienceDirect

journal homepage: www.elsevier.com/locate/carbon

Water condensation behavior on the surface of a network of superhydrophobic carbon fibers with high-aspect-ratio nanostructures

Tae-Jun Ko [a,b], Eun Kyu Her [a,b], Bongsu Shin [b,c], Ho-Young Kim [c], Kwang-Ryeol Lee [b], Bo Ki Hong [d], Sae Hoon Kim [d], Kyu Hwan Oh [a], Myoung-Woon Moon [b,*]

[a] Department of Materials Science and Engineering, Seoul National University, Seoul 151-742, Republic of Korea
[b] Future Conversion Technology Research Division, Korea Institute of Science and Technology, Seoul 130-650, Republic of Korea
[c] School of Mechanical and Aerospace Engineering, Seoul National University, Seoul 151-742, Republic of Korea
[d] Fuel Cell Vehicle Team 1, Eco-Technology Center, Hyundai-Kia Motors, Yongin-Si, Gyeonggi-Do 446-912, Republic of Korea

ARTICLE INFO

Article history:
Received 3 May 2012
Accepted 25 June 2012
Available online 2 July 2012

ABSTRACT

We have explored the condensation behavior of water on a superhydrophobic carbon fiber (CF) network with high-aspect-ratio hair-like nanostructures. Nanostructures ranging from nanopillars to hairy shapes were grown on CFs by preferential oxygen plasma etching. Superhydrophobic CF surfaces were achieved by application of a hydrophobic siloxane-based hydrocarbon coating, which increased the water contact angle from 147° to 163° and decreased the contact angle hysteresis from 71° to below 5°, sufficient to cause droplet roll-off from the surface. Water droplet nucleation and growth on the superhydrophobic CF were significantly retarded due to the high-aspect-ratio nanostructures under super-saturated vapor conditions. CFs are observed to wet with condensation between fibers of the pristine surface under super-saturated vapor conditions, which eventually leads to flooding. However, dropwise condensation became dominant in the superhydrophobic CF network, allowing for easy removal of the condensed droplets, which largely allowed the interstitial spaces of the fiber network to remain dry. It is implied that superhydrophobic CF can provide a passage for vapor or gas flow in wet environments such as a gas diffusion layer requiring the effective water removal in the operation of proton exchange membrane fuel cell.

1. Introduction

Numerous studies have been conducted on the unique characteristics of carbon fiber (CF) such as high strength, light weight, and high porosity, which are applicable in various fields ranging from conventional areas such as aircraft, automobile, and sports [1,2] to more recent energy storage and transfer technologies such as electrodes for super-capacitor [3,4] and lithium ion batteries [5,6] and gas diffusion layer (GDL) for proton exchange membrane fuel cell (PEMFC) [7]. Especially, GDL is composed of microscale CF networks such as CF-felt, paper, or cloth, and that provides the microscale porosity which allows for effective flow of reactant gases in PEMFC. However, during the PEMFC operation, water is generated from the oxygen reduction reaction, and sometime excessive water is condensed on CF network, which would block the transition sites of CF networks of GDL, resulting in water flooding. This phenomenon inhibits the transport of

* *Corresponding author:* Fax: +82 2 958 5487.
E-mail address: mwmoon@kist.re.kr (M.-W. Moon).
0008-6223/$ - see front matter
http://dx.doi.org/10.1016/j.carbon.2012.06.048

oxygen and raises the voltage loss [8]. For that reason, a higher hydrophobic CF network has been adopted for GDL to suppress the water condensation and to remove condensed water easily during cell operation [7,9–11]. Although a lot of studies have been conducted to introduce hydrophobic materials such as polytetrafluoroethylene (PTFE) or surface treatments with CF_4, CHF_3, or SF_6 plasma to improve the hydrophobicity of CF network in GDL, suppressing of water condensation and effective water removal by management of excessive liquid water condensation in CF networks still remains a major challenge in research of GDL [10,11].

Superhydrophobicity has been commonly defined by a high contact angle of a surface with a water droplet exceeding 150° and a low hysteresis of the difference in the advancing and receding angle for the droplet. To release condensed water from a surface, these properties can be achieved by a compound micro- and nanoscale roughness combined with a low-energy material coating on structures such as metals, semiconductors, or curved woven or non-woven fiber structures [12,13]. In the case of CF networks, various bottom-up techniques have been employed for enhancing hydrophobicity to fabricate nanostructures with additional roughness of the CFs. Nanostructures such as carbon nanotubes or carbon nanofibers have been fabricated on top of CF networks for water repellency using chemical vapor methods [14,15]. However, a recent study revealed that despite water-repellent behavior with respect to millimeter-scale water droplets, the surfaces can lose their water-repellent properties during vapor condensation, which should be considered a micrometer-scale water nucleation and growth problem. Cheng et al. revealed the importance of robustness to vapor condensation in superhydrophobicity by showing that the lotus leaf, a well-known superhydrophobic surface with hierarchical roughness in the micro- and nanoscales covered with a wax coating, loses its water-repellent properties after water vapor condensation on its surface [16]. Recently, Shin et al. reported that superhydrophobic surfaces with high-aspect-ratio nanostructures exhibited water repellency with the ability to roll off condensed water vapor droplets while superhydrophobic surfaces with low-aspect-ratio nanostructures did not sustain their water repellency in the same conditions [17]. These results therefore suggest that not only superhydrophobicity but also the aspect ratio of a nanoscale pattern may be crucial factors for consideration to allow the removal of condensed water on CF networks.

In this work, we fabricated CF network surfaces with high-aspect-ratio nanostructures having superhydrophobic and water-repellent properties which suppress the water condensation as well as remove the condensed water easily. The aspect ratios of nanostructures on CF networks were controlled with oxygen plasma etching, an economical and eco-friendly method, after which a subsequent hydrophobic coating treatment rendered the superhydrophobic CF networks shown in Fig. 1. The formation mechanism of the nanostructures was explored by measurement of the changes in CF surface chemistry before and after oxygen plasma treatment using X-ray photoelectron spectroscopy (XPS). The water contact angle (CA) and contact angle hysteresis (CAH), defined as the difference between the advancing angle during water deposition and receding angle during water removal, were measured at

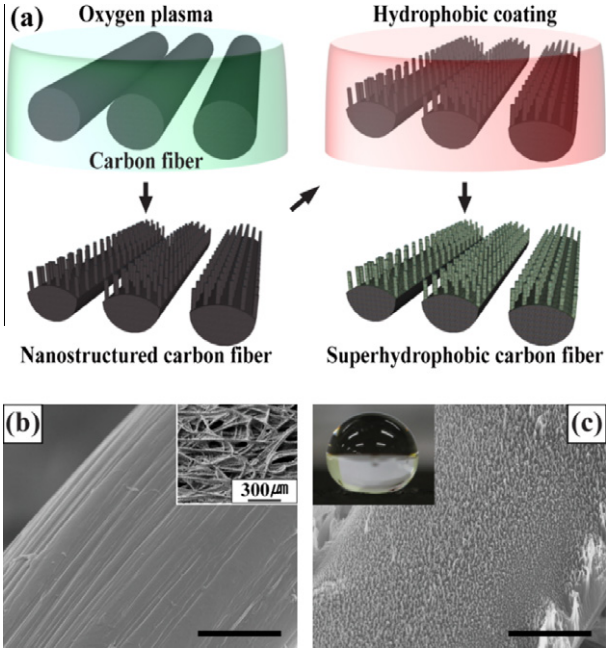

Fig. 1 – (a) A schematic for CF plasma etching and subsequent coating with hydrophobic HMDSO. SEM images of CFs (b) before and (c) after nanostructuring by oxygen plasma etching. The scale bars in (b) and (c) are 2 μm. The insets are a low-magnification image of CF networks (b) and an optical image of a spherical droplet of water (c).

ambient room temperature and at 80 °C, which is close to the operating temperature of a PEMFC [7,9]. The water droplet nucleation and growth were investigated by environmental scanning electron microscope (ESEM) in super-saturated vapor conditions on nanostructured CF networks and organized according to structure aspect ratios. The Laplace pressure of the droplets as well as the water-covered area fraction was estimated on each CF nanostructure aspect ratio.

2. Experimental

2.1. *Preparation of superhydrophobic CF network*

To fabricate superhydrophobic nanostructured surfaces, oxygen plasma etching and coating with hydrophobic material were applied to CFs made of carbonized polyacrylonitrile (PAN) that were 8–10 μm in diameter supported by carbon patches that are mainly composed of carbon powders with 1–10 μm in width and length to improve the electrical conductivity of the GDL. Fig. 1a shows a schematic for the fabrication of superhydrophobic surfaces on the CF networks that have randomly oriented CFs and carbon patches between the fibers, as shown in the inset of Fig. 1b. Oxygen plasma etching was performed to form the nanostructures on the CFs, and hydrophobic material coating was accomplished with radio-frequency plasma-enhanced chemical vapor deposition (r.f.-PECVD) system. The aspect ratios were controlled by the oxygen plasma treatment duration (in the range of 1–60 min) with a bias voltage of −400 V. Three different working

pressures (5, 10 and 30 mTorr) were also used to explore the effect of working pressure on the fiber surface patterns. A hydrophobic SiO_x–C:H coating derived from a hexamethyldisiloxane (HMDSO) precursor vapor (Sigma Aldrich), which has a low surface energy (24 mN/m), was coated on surfaces of pristine and nanostructured CF networks [18–20]. For the SiO_x–C:H coating, a bias voltage of −400 V, working pressure of 10 mTorr and a 30 s duration typically resulted in a coating that was 30 nm thick.

2.2. SEM, XPS analysis & contact angle measurement

A scanning electron microscope (SEM, FEI, Nova NanoSEM 200) with a 10 kV electron acceleration voltage was used to examine the surface morphology of the samples. Both the top view and 30° tilting view were employed to measure the aspect ratio (a ratio of the height to the diameter) of nanostructure. X-ray photoelectron spectroscopy (XPS, ESCA System, PHI 5800) was also used to compare the chemical bonding of the CFs before and after oxygen plasma treatment. Water wettability of the pristine and the superhydrophobic CF networks was characterized by measuring the CA and the CAH of de-ionized water with a sessile drop test. The approximately 5 μL droplets were gently deposited on the CF network surfaces using a microsyringe. The CA and the CAH values were measured using a goniometer (Rame-Hart) in ambient air at a relative humidity of 20–35% at 20 and 80 °C.

2.3. Observation of water condensation behavior in ESEM

An environmental scanning electron microscope (ESEM, FEI, XL-30 FEG) was used to examine the water condensation, growth and repellency behaviors of the nanostructured CF networks. The ESEM images were taken every 15 s as the chamber pressure was increased from 3.0 to 5.8 Torr, which, at the 2 °C maintained by a cold stage module, corresponds to a transition from under-saturation to over-saturation. To measure the water droplet radii and water-covered area fraction, we carried out rough observation using ESEM images which were taken at a 45° tilting angle view. The area covered by condensed water on the $712 \times 484\ \mu m^2$ area shown in ESEM images was estimated by counting pixels in the images which were taken at least 8 times at different areas. The Laplace pressure of smaller spherical droplets on each CF networks was calculated and correlated with the surface structure aspect ratio.

3. Results and discussion

3.1. Characterization of surface morphology

CF networks were subjected to different oxygen plasma treatment duration, and the formed various nanostructures can be observed as shown in Fig. 2. As the plasma treatment duration increased, the configuration of the structures changed from nanopillars to hairy structures, with a significant increase in the nanostructure length from 9.8 to 1061 nm and a smaller increase in the diameter from 10.0 to 28.4 nm as shown in Fig. 2a–e. The aspect ratio increased to greater than 30 at 10 mTorr with increasing plasma treatment duration, as shown in Fig. 2f. For short treatment duration between 1 and 5 min at 10 mTorr, the structure began to evolve from a low aspect ratio, which increased as the plasma duration exceeded 15 min, ultimately forming nanostructures with aspect ratios of up to 37 on CFs at a treatment duration of 60 min. The etching rate was lower at a 5 mTorr working pressure than at 10 mTorr. Because of the higher etching rate at 30 mTorr, the aspect ratios at short plasma treatment duration were higher

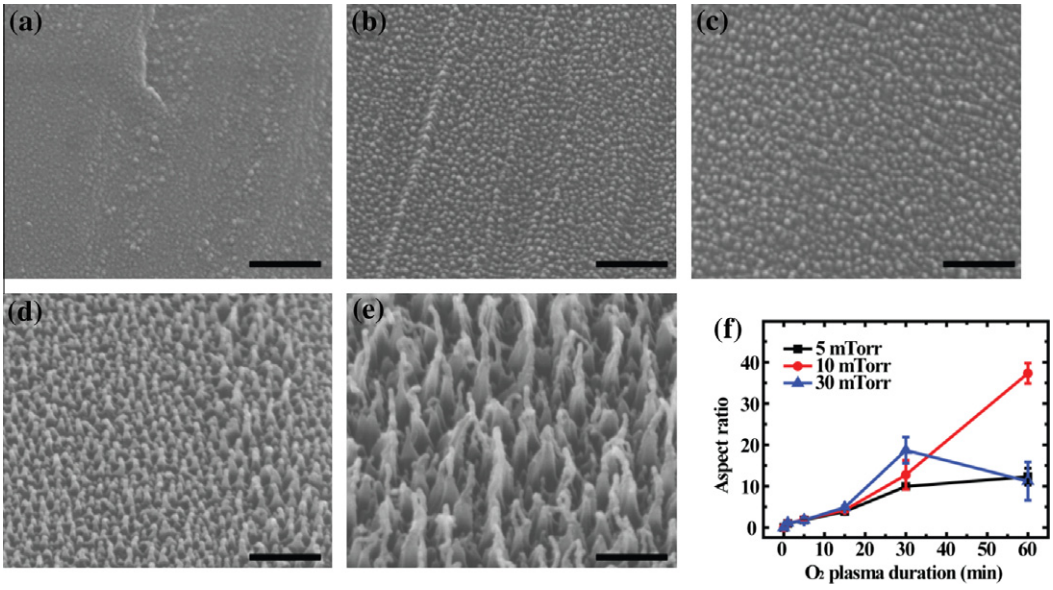

Fig. 2 – SEM images of nanostructures formed on CFs when treated by different oxygen plasma etching duration at 10 mTorr for (a) 1, (b) 5, (c) 15, (d) 30, and (e) 60 min. The scale bars in (a–e) are 200 nm. (f) A graph of the nanostructure aspect ratio on CFs with respect to the plasma treatment duration at three chosen working pressures. The aspect ratio was estimated from the images taken by SEM.

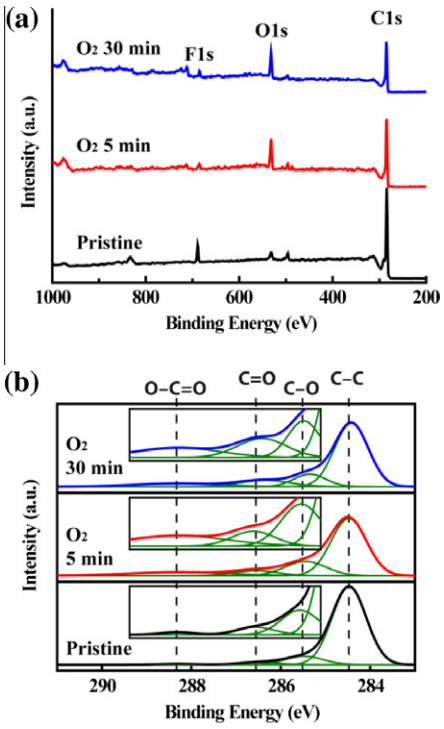

Fig. 3 – (a) Low-resolution and (b) high-resolution C1s survey XPS spectra before and after oxygen plasma treatment (duration of 5 and 30 min at 10 mTorr).

than those at 10 mTorr but were reduced due to over-etching for etching duration of greater than 30 min.

3.2. *Analysis using X-ray photoelectron spectroscopy*

CF surfaces before and after oxygen plasma etching were characterized by XPS; the spectra are shown in Fig. 3. The XPS spectrum oxygen peaks increased in strength after oxygen plasma treatment as shown in Fig. 3a and Table 1, while the concentration of carbon atoms decreased after oxygen plasma exposure. More specifically, the oxygen concentration increased from 3.3% to 13.9% after a 1 min oxygen plasma treatment. Additionally, it was noted that the concentrations of carbon and oxygen atoms are gradually increased between 1 and 60 min of oxygen plasma treatment.

The C1s XPS peaks were used to analyze the bonding information, as shown in Fig. 3b. The C1s peaks were deconvoluted to four Gaussian peaks at 284.5 (C–C bond), 285.5 (C–O bond), 286.5 (C=O bond), and 288.3 eV (O–C=O bond) [21]. The peaks for the 5 min oxygen plasma-treated fibers show a broad shoulder towards higher binding energy that is related to oxygen-containing species. During the oxygen plasma treatment, oxygen atoms may break C–C bonds in the CFs and bind the unbonded carbon atoms to form functional groups. The functional groups formed on the CFs are listed in Table 2. It is revealed that the number of functional groups increased significantly as a consequence of a 1 min oxygen plasma treatment. These results were similar to those for the 60 min treatment, which indicates that active sites on the CF may have become saturated during the early stages of plasma treatment [21] and the rate of formation of additional functional groups becomes equal to the etching rate [22].

The formation of nanostructures on the CF by oxygen plasma is believed to be due to the preferential etching of defect parts over the crystalline structure in the CF. It has been reported that the CF is composed of graphitic regions and low-ordered regions with defects or pores [23–26]. These low-ordered regions in the CFs would be oxidized faster by oxygen plasma as well as have a lower resistance to etching. Furthermore, it was reported that the preferential etching on less ordered regions increases their oxygen content, which further accelerates the local etching rate [27,28]. Thus, it could be understood that during the oxygen plasma treatment, the low-ordered regions of the surface between the highly ordered graphitic regions are preferentially etched while graphitic regions would be less etched, which results in the formation of surface nanostructures [25,27–30].

3.3. *Contact angle measurement with sessile drop test*

The water wetting behavior was characterized by measurement of CA and CAH on the CF networks at two different temperature conditions at 20 and 80 °C. Due to the microstructure consisting of the CF, a pristine CF network had a high water CA (147°) and also a high CAH (71°), which is insufficient to cause the water droplet to roll off the surface. As a result, sessile water droplets on the pristine surfaces had low mobility and were pinned on the CF network surface even after the surface was tilted 90° relative to the ground, as shown in Fig. 4a. However, the surface treated for 60 min with oxygen plasma and 30 s for the hydrophobic SiO_x–C:H coating showed a relatively higher water CA (162°) as well as a low CAH (below than 5°), which is sufficient to cause droplet roll off from the surface at very slight tilting angles (less than 5°), as shown in the images of Fig. 4b. These results indicate that nanostruc-

Table 1 – Atomic concentration (at.%) and atomic ratio of oxygen plasma-treated CFs.

O_2 plasma duration (min)	Atomic concentration, in%			Atomic ratio
	C	O	F	O/C
Pristine	91.9	3.3	4.8	0.04
1	82.5	13.9	1.4	0.17
5	81.8	14.9	1.6	0.18
15	79.1	15.7	3.1	0.20
30	77.5	18.2	2.7	0.23
60	74.8	19.4	4.4	0.26

Table 2 – Relative amount (%) of functional groups in C1s peak of oxygen plasma-treated CF.

O_2 plasma duration (min)	Relative amount, in%			
	C–C (284.5 eV)	C–O (285.5 eV)	C=O (286.5 eV)	O–C=O (288.3 eV)
Pristine	85.7	10.3	3.1	0.9
1	70.3	14.2	8.9	6.6
5	68.0	14.7	10.3	7.0
15	67.4	16.2	9.0	7.4
30	63.4	18.4	8.9	9.3
60	64.9	13.4	11.2	10.5

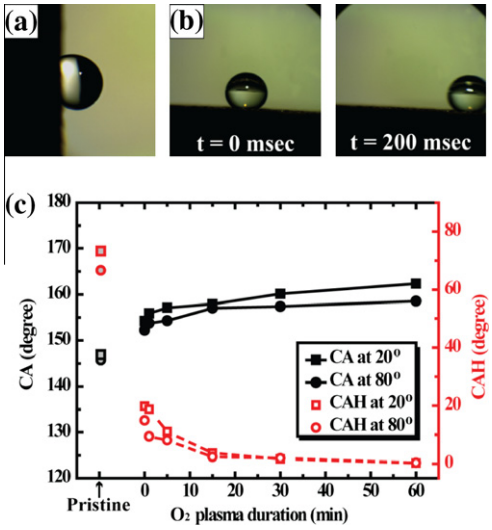

Fig. 4 – Contact angle behavior of water droplets on (a) pristine CFs and (b) superhydrophobic CFs plasma-treated for 60 min at 10 mTorr. (c) Evolution of water droplet CA and CAH with respect to the oxygen plasma treatment duration.

tured and hydrophobic material-coated CF network surfaces enhance the hydrophobicity and result in water repellency for sessile droplets.

It is known that introducing surface roughness enhances the existing hydrophilicity or hydrophobicity of the material [12,13,17]. With a low-surface-energy material coating on the nanostructured fiber surfaces, wetting properties can be enhanced from hydrophobic to superhydrophobic. This rule can be explained by Cassie's law in Eq. (1), which describes the effective contact angle θ_c for a liquid on a composite surface as

$$\cos\theta_c = f_1\cos\theta_1 + f_2\cos\theta_2 \quad (1)$$

where θ_c is the apparent CA, θ_1 is the CA for component 1 with area fraction f_1 and θ_2 is the CA for component 2 with area fraction f_2 in the composite material. When the second component is air (with a CA of 180°), Eq. (1) can be reduced to

$$\cos\theta_c = f_1(\cos\theta_1 + 1) - 1 \quad (2)$$

When a water droplet is deposited on a nanostructured surface with a contact area fraction of f_1, the equilibrium condition for the water droplet can be regarded as a Cassie–Baxter state. Eq. (2) indicates that as the fraction of contact area decreases, hydrophobicity can be enhanced on the structure. In this context, longer oxygen etching duration, which results in a nanostructure with higher aspect ratio on the CFs, also significantly reduces the CF contact area fraction from 11% up to 5%, which was calculated using Eq. (2) by referring previous work [18]. The evolution of the CA and CAH was traced by varying the oxygen plasma duration and measuring the CA and CAH at different surface temperatures. The results are shown in Fig. 4c. The pristine fiber network with a CA of 147° presents a hydrophobic nature owing to its microscale fibrous network structure, with large pore areas between fibers. After hydrophobic SiO_x–C:H treatment of a pristine CF network, the CA increased from 147° to 155° and the CAH decreased from 71° to 20°. Upon plasma treatment at increasingly longer treatment duration (followed by SiO_x–C:H treatment), the CF network CA measured at 20 °C increased up to 160° with a very low CAH of less than 5°; similar CA and CAH behaviors were shown for the samples measured at 80 °C.

3.4. *Water condensation behavior on nanostructured CF network*

In the static CA and CAH sessile droplet test, the hydrophobicity of macroscale sessile droplets was improved and water repellency was observed for the CFs with nanostructure aspect ratios of greater than 4.2. However, as discussed earlier in this work, the wetting behavior of 1 mm radius droplets in the sessile droplet test would be quite different from that of water droplets nucleated and grown on the surface because of their much smaller radius. Fig. 5 shows how water droplets grow and coalesce on CF surfaces with different surface structures developed via plasma treatment and hydrophobic material coating. ESEM observations were performed on three different samples: a pristine sample and two samples that underwent 15 and 60 min of oxygen plasma treatment with subsequent hydrophobic coating. It is noted that both CF networks treated in such a manner exhibited superhydrophobicity with CAs of greater than 150° and very low CAH (see Fig. 4c). In the pristine CF surface (Fig. 5a), small water droplets with diameters less than 10 μm initially appeared on the CFs as the vapor pressure increased from 3.0 to 5.8 Torr. As the sample was held at 5.8 Torr for up to 300 s, the water droplets that formed on the CFs gradually increased in diameter to over 40 μm with a CA less than 90°. Small droplets (denoted number 1–3 in Fig. 5a) started to increase in size and merged with neighboring water droplets. In the final stage of

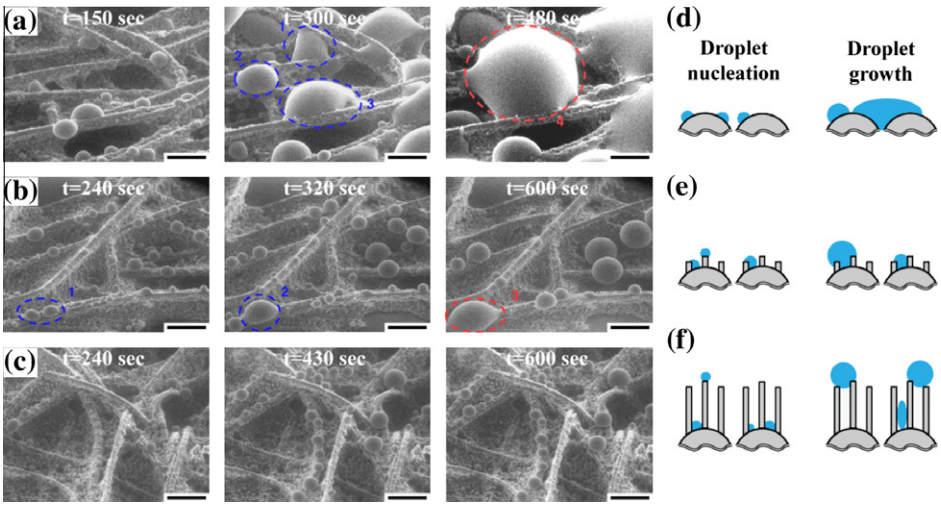

Fig. 5 – ESEM images on three different fiber surfaces: (a) pristine, (b) 15 min plasma-treated and 30 s hydrophobic film-coated and (c) 60 min plasma-treated and 30 s hydrophobic film-coated surfaces (Scale bars are 50 μm). (d–f) Schematics regarding the condensation of water with respect to the aspect ratio of nanostructures formed on the CFs.

condensation, the droplets located on different fibers coalesce together to become one big droplet (denoted number 4 in Fig. 5a) with a diameter greater than 50 μm, which formed a "water bridge" across the CFs. With longer duration at the 5.8 Torr pressure, the coalesced droplets formed water films bridging across the pore sites between the fibers and finally caused water flooding over the pristine CF network. Fig. 5b shows the condensation behavior of the superhydrophobic CF surface with a relatively low aspect ratio of 4.2, created during the oxygen plasma treatment for 15 min. In the initial stages, the droplets appeared relatively hydrophobic, and dropwise condensation around the CFs occurred under super-saturated vapor upon increase of the water vapor pressure. For duration up to 320 s at 5.8 Torr, some droplets (denoted number 1 in Fig. 5b) were observed to grow on the fibers and coalesced with neighboring smaller droplets to form larger droplets (denoted numbers 2, 3 in Fig. 5b). On the superhydrophobic CF surface with relatively low aspect ratios, even though the overall size of the droplets is smaller than those of droplets on the pristine CFs in Fig. 5a, smaller droplets were shown to be pinned on the fibers and had low mobility. On the superhydrophobic fiber surface with an aspect ratio of 37, achieved by a 60 min oxygen plasma treatment as shown in Fig. 5c, a number of tiny water droplets were nucleated on the CFs in the early stages, but maintained their spherical shape. During the growth stage, droplets tend not to coalesce with each other easily, with a relatively small diameter of less than 10 μm. These results indicate that superhydrophobic surfaces composed of higher-aspect-ratio nanostructures maintain their hydrophobicity, with a low tendency for condensed water droplets to coalesce.

During the condensation stage, droplets on the pristine CFs may nucleate either on or between the fibers; they then grow further and coalesce with neighboring droplets. Fig. 5d shows that on the pristine CF, condensed water droplets grew in a relatively low-CA environment. As the droplets merge with each other, they begin to contact larger areas of CFs, resulting in it becoming more difficult to move from the CF network and become more easily merged with neighboring droplets, which results in blocking of the interstitial spaces between fibers. However, on the nanostructured superhydrophobic surfaces with smaller aspect ratios, water droplet nucleation sites are distributed not only on the top of the structure but also in the spaces between structures. Upon condensation, both of the droplets grow and coalesce with each other, which results in the formation of larger water droplets on the surfaces with low-aspect-ratio nanostructures (Fig. 5e). As the water droplets grow on top of the surface features, they also penetrate between the structures and are pinned by the contact line, decreasing droplet mobility and increasing CAH [31,32], similar to the wetting behavior of condensed water on the lotus leaf [16]. However, on the superhydrophobic CF networks with high-aspect-ratio nanostructures, a nucleated droplet can maintain its spherical shape and have a difficulty to merge with other droplets that nucleate in the structure spaces as shown in Fig. 5f. These phenomena decrease the possibility of transition from the Cassie–Baxter to Wenzel regimes under the super-saturated vapor conditions [17]. The droplet can thus be released from the fiber spontaneously because Cassie–Baxter state droplets have lower hysteresis, and the chances for blocking the interstitial spaces between the fibers decreases dramatically.

Superhydrophobic CF networks allow not only dropwise condensation but also suppressing of the water droplet nucleation. In our work, condensed droplets were observed to form after 90 s on pristine CF at a vapor pressure of 5.8 Torr, while they appeared after 220 s on the superhydrophobic CFs with a 60 min plasma treatment duration. In other words, the water droplet nucleation rate becomes lower significantly in the case of the superhydrophobic CF surface than that on the pristine surface; Sigsbee's equation, including the rate of heterogeneous nucleation as a function of the contact angle and the surface tension, is adopted as follows [17,33,34]:

$$J = J_0 \exp(-\Delta G/kT) = J_0 \exp[-\pi\gamma r^{*2}(2 - 3\cos\theta + \cos^3\theta)/3kT] \quad (3)$$

where J is the nucleation rate, J_0 is a kinetic constant, γ is the liquid–vapor surface energy per unit area, r^* is the critical radius, θ is the equilibrium CA, k is the Boltzmann constant and T is the absolute temperature. Eq. (3) shows that the nucleation rate of water droplet may decrease with increases in CA or θ because the nucleation energy barrier increases. In the case of the superhydrophobic CF network, nucleation sites at the top parts of the nanostructure are much smaller than those on the pristine fiber network. With the low nucleation rate and the dropwise condensation behavior on the superhydrophobic CFs, droplet coalescence tends to decrease and interstitial spaces between the CFs remain dry.

To quantify the condensation behavior according to the aspect ratio of nanostructures, the Young–Laplace equation is adopted to relate the pressure difference (Δp) across the gas–liquid interface to the surface tension and the interface curvature [17,35]. Especially in the case of a sessile droplet shaped as a sphere, the pressure difference between the inside and outside of the droplet can be stated as $\Delta p = 2\gamma/R$, where R is the principal radius of curvature of the droplet. From the images taken by ESEM, the measured radii for small droplets formed on fiber networks was used for the calculation of the Young–Laplace pressure (Δp) of the water droplet on the CF surface as shown in Fig. 6a. The maximum pressure can be calculated by measurement of the smallest nucleated drop radius. On the pristine CFs, the Laplace pressure is estimated to be as high as 6.8 kPa. However, superhydrophobic nanostructured CFs can maintain Laplace pressures from 10.5 to 52.4 kPa, as the nanostructure aspect ratio increases upon increasing the oxygen plasma treatment duration.

To examine the ability of the superhydrophobic CF network surface to prevent water film formation, the water-covered area fraction (the fraction of area covered by water divided by the projected area) was estimated from the ESEM images taken with the increase in pressure holding duration, as shown in Fig. 6b. Films of water began to form on the pristine surface over 8.8% of the area at 240 s, and their area fraction increased up to 94.2% at 600 s at 5.8 Torr. This high water-film formation rate and relatively early formation of a water film originated from the low CA and high nucleation rate due to low hydrophobicity. However, in superhydrophobic nanostructured CF networks, after 600 s at a vapor pressure of 5.8 Torr, films made without oxygen plasma treatment were covered by water films on over 46.9% of their surface, and this fraction decreased to 0.4% as the oxygen plasma duration was increased to 60 min. As discussed above, superhydrophobic surfaces with higher nanostructure aspect ratios would sustain the high liquid pressure and hinder water film formation, which is helpful in preventing flooding of CF networks with high-aspect-ratio nanostructures.

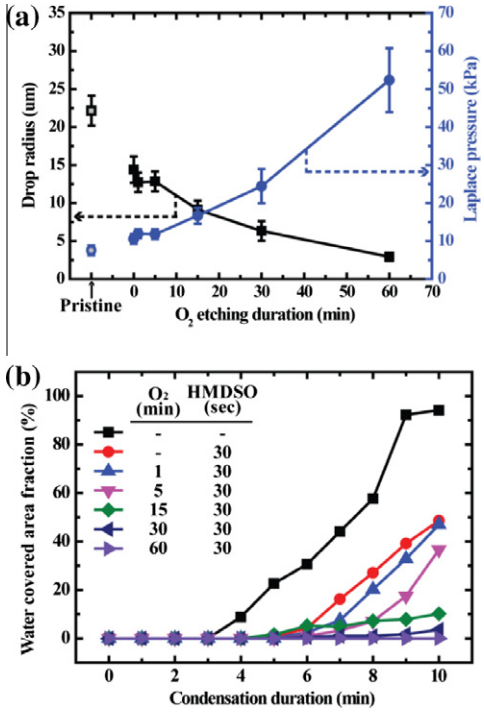

Fig. 6 – (a) Graph of the measurement of droplet radius and Laplace pressure with respect to the oxygen plasma duration. (b) Water-covered area fraction measured on the CFs according to different surface treatment conditions, recorded with ESEM. Both of drop radius and water-covered area fraction were measured by rough observation using ESEM.

4. Conclusion

Superhydrophobic and highly water-repellent properties characterized by a lower rate of water droplet nucleation were enabled on nanostructured CF networks using oxygen plasma etching and subsequent low-energy material coating via an r.f.-PECVD technique. The processing enables us to control and create aspect ratios up to 37 by extending the plasma duration up to 60 min. In the sessile water droplet test, nanostructured CFs have a CA higher than 150° and a CAH less than 10° in ambient temperature as well as at 80 °C. Furthermore, due to their high aspect ratio, nanostructured CFs with superhydrophobicity have the spherical shape produced by dropwise condensation, which could be maintain under Laplace pressures of up to 52.4 kPa. The nucleation rate of water droplets was significantly suppressed, and the time required until the first droplet appearance was 244% longer compared to that for pristine CFs. The repellent behavior that protects against formation of a water film was enhanced to achieve 0.4% of area fraction on a superhydrophobic CF network surface, while water covered 94.2% of a pristine CF network surface after 600 s at a vapor pressure of 5.8 Torr. The water removal rate on GDL surfaces was improved enough to prevent flooding by applying superhydrophobic CFs with high-aspect ratio-nanostructures. Moreover, such nanostructuring of carbon-based materials can be extended to CFs, carbon black or carbon films for applications as a cathode in lithium batteries or CF composites.

Acknowledgements

This study was financially supported in part by the MKE (10040003), Korea (M.W.M.), Hyundai-Kia Motors Co. and KIST and in part by the National Research Foundation of Korea (NRF) funded by the Ministry of Education, Science and Tech-

nology (R11-2005-065, K.H.O.). H.Y.K. acknowledges administrative support of SNU-IAMD.

REFERENCES

[1] Thostenson ET, Li WZ, Wang DZ, Ren ZF, Chou TW. Carbon nanotube/carbon fiber hybrid multiscale composites. J Appl Phys 2002;91(9):6034–7.

[2] Bekyarova E, Thostenson ET, Yu A, Kim H, Gao J, Tang J, et al. Multiscale carbon nanotube-carbon fiber reinforcement for advanced epoxy composites. Langmuir 2007;23(7):3970–4.

[3] Hu C-C, Li W-Y, Lin J-Y. The capacitive characteristics of supercapacitors consisting of activated carbon fabric–polyaniline composites in $NaNO_3$. J Power Sources 2004;137(1):152–7.

[4] Kalinathan K, DesRoches DP, Liu XR, Pickup PG. Anthraquinone modified carbon fabric supercapacitors with improved energy and power densities. J Power Sources 2008;181(1):182–5.

[5] Endo M, Kim C, Nishimura K, Fujino T, Miyashita K. Recent development of carbon materials for Li ion batteries. Carbon 2000;38(2):183–97.

[6] Endo M, Kim YA, Hayashi T, Nishimura K, Matusita T, Miyashita K, et al. Vapor-grown carbon fibers (VGCFs) – basic properties and their battery applications. Carbon 2001;39(9):1287–97.

[7] Li H, Tang YH, Wang ZW, Shi Z, Wu SH, Song DT, et al. A review of water flooding issues in the proton exchange membrane fuel cell. J Power Sources 2008;178(1):103–17.

[8] Saleh MM, Okajima T, Hayase M, Kitamura F, Ohsaka T. Exploring the effects of symmetrical and asymmetrical relative humidity on the performance of H2/air PEM fuel cell at different temperatures. J Power Sources 2007;164(2):503–9.

[9] Shimpalee S, Beuscher U, Van Zee JW. Analysis of GDL flooding effects on PEMFC performance. Electrochim Acta 2007;52(24):6748–54.

[10] Pai YH, Ke JH, Huang HF, Lee CM, Jyh-Myng Z, Shieu FS. CF4 plasma treatment for preparing gas diffusion layers in membrane electrode assemblies. J Power Sources 2006;161(1):275–81.

[11] Lee CM, Pai YH, Zen JM, Shieu FS. Characterization of Teflon-like carbon cloth prepared by plasma surface modification for use as gas diffusion backing in membrane electrode assembly. Mater Chem Phys 2009;114(1):151–5.

[12] Lafuma A, Quere D. Superhydrophobic states. Nat Mater 2003;2(7):457–60.

[13] Quéré D. Wetting and roughness. Annu Rev Mater Res 2008;38:71–99.

[14] Wang C, Waje M, Wang X, Tang JM, Haddon RC, Yan YS. Proton exchange membrane fuel cells with carbon nanotube based electrodes. Nano Lett 2004;4(2):345–8.

[15] Hsieh CT, Chen WY. Water/oil repellency and drop sliding behavior on carbon nanotubes/carbon paper composite surfaces. Carbon 2010;48(3):612–9.

[16] Cheng YT, Rodak DE, Angelopoulos A, Gacek T. Microscopic observations of condensation of water on lotus leaves. Appl Phys Lett 2005;87(19):194112.

[17] Shin B, Lee K-R, Moon M-W, Kim H-Y. Extreme water repellency of nanostructured low-surface-energy non-woven fabrics. Soft Matter 2012;8(6):1817–23.

[18] Rahmawan Y, Moon M-W, Kim K-S, Lee K-R, Suh K-Y. Wrinkled, dual-scale structures of diamond-like carbon (DLC) for superhydrophobicity. Langmuir 2009;26(1):484–91.

[19] Her EK, Ko T-J, Lee K-R, Oh KH, Moon M-W. Bioinspired steel surfaces with extreme wettability contrast. Nanoscale 2012;4(9):2900–5.

[20] Kim T-Y, Ingmar B, Bewilogua K, Oh KH, Lee K-R. Wetting behaviours of a-C:H:Si:O film coated nano-scale dual rough surface. Chem Phys Lett 2007;436(1–3):199–203.

[21] Jin BS, Lee KH, Choe CR. Properties of carbon-fibers modified by oxygen plasma. Polym Int 1994;34(2):181–5.

[22] Jones C, Sammann E. The effect of low power plasmas on carbon fibre surfaces. Carbon 1990;28(4):509–14.

[23] Mathias MF, Roth J, Fleming J, Lehnert W. Diffusion media materials and characterization. In: Vielstich W, Gasteiger HA, Lamm A, editors. Handbook of fuel cells-fundamentals, technology and applications, vol. 3. New York: John Wiley and Sons; 2003. p. 517–37.

[24] Zhou G, Liu Y, He L, Guo Q, Ye H. Microstructure difference between core and skin of T700 carbon fibers in heat-treated carbon/carbon composites. Carbon 2011;49(9):2883–92.

[25] Hoffman WP, Hurley WC, Owens TW, Phan HT. Advantage of the scanning tunneling microscope in documenting changes in carbon-fiber surface-morphology brought about by various surface treatments. J Mater Sci 1991;26(17):4545–53.

[26] Riggs JP. Carbon fibers. In: Mark HF, Bikales NM, Overberger CG, Menges G, editors. Encyclopedia of polymer science and engineering, 2nd ed., vol. 2. New York: John Wiley and Sons; 1985. p. 640–85.

[27] Boudou JP, Paredes JI, Cuesta A, Martinez-Alonso A, Tascon JMD. Oxygen plasma modification of pitch-based isotropic carbon fibres. Carbon 2003;41(1):41–56.

[28] Paredes JI, Martinez-Alonso A, Tascon JMD. Oxygen plasma modification of submicron vapor grown carbon fibers as studied by scanning tunneling microscopy. Carbon 2002;40(7):1101–8.

[29] Barnet FR, Norr MK. Carbon fiber etching in an oxygen plasma. Carbon 1973;11(4):281–8.

[30] Junkar I, Cvelbar U, Vesel A, Hauptman N, Mozetic M. The role of crystallinity on polymer interaction with oxygen plasma. Plasma Process Polym 2009;6(10):667–75.

[31] Jung YC, Bhushan B. Wetting behaviour during evaporation and condensation of water microdroplets on superhydrophobic patterned surfaces. J Microsc 2008;229(Pt 1):127–40.

[32] Wier KA, McCarthy TJ. Condensation on ultrahydrophobic surfaces and its effect on droplet mobility: ultrahydrophobic surfaces are not always water repellant. Langmuir 2006;22(6):2433–6.

[33] Zhao H, Beysens D. From droplet growth to film growth on a heterogeneous surface – condensation associated with a wettability gradient. Langmuir 1995;11(2):627–34.

[34] Varanasi KK, Hsu M, Bhate N, Yang WS, Deng T. Spatial control in the heterogeneous nucleation of water. Appl Phys Lett 2009;95(9):094101–94103.

[35] Ouyang G, Wang CX, Yang GW. Surface energy of nanostructural materials with negative curvature and related size effects. Chem Rev 2009;109(9):4221–47.